Meniscal boron addition, such as in AISI 316L stainless steel, is sufficient to improve sintering. The addition of boron affects the sintered compacts property, resulting in a nearly continuous chain of solidified brittle eutectic phase encircling the grains, in addition to the significant positive improvements in sintering stainless steel powders. Only when the sinter's nature is continuous does this reduce its mechanical qualities. The loss of mechanical qualities is permissible when the network transforms into dispersed and discontinuous precipitations [9,10]. The shape, amount and size of precipitations can be changed by managing the sintering process and establishing the suitable temperature profile, sintering environment, and chemical composition [11,12]. The results obtained after sintering electrolytic grade iron particles with boron powders are presented in this paper.

Materials and Methods

Pure iron powders of electrolytic grade were used. Boron powders with a particle size of 200 mesh were employed, which were 99% pure. Table 1 shows the chemical composition and basic properties of iron particles. In a RETSCH high energy ball mill with hardened chrome steel container and balls, both pure iron powders and 1% boron alloyed powders were homogenized and processed. Total weight of 100 gm of balls (8 mm diameter) was used, with a ball to powder weight ratio of 2:1. During mixing and milling, the speed was kept at 100 rpm and 400 rpm, respectively. The grinding was completed and the powders were collected at 3, 6, 9 and 12 hours intervals, respectively. Wet milling was done using toluene.

Sintering in a vacuum was achieved by encapsulating powders in a quartz tube using glass blowing. Sintering was placed for 45 minutes in a high temperature muffle furnace at 1200°C. The sintering temperature was reached at a rate of -15 K/min, while the cooling rate was -10 K/min. Scanning electron microscopy was used to examine the microstructure of specimens (JSM-5600 LV and JSM-6700 F). A Philips CM200 transmission electron microscope operating at 200 kV was used to perform energy dispersive spectroscopy. The spectra were taken using a windowless detector and analyzed with the ES vision 3.0 software. X-Ray Diffraction (XRD, diffractometer-6000, 40 kV, 30 mA, Cu, K) was used to evaluate the phase compositions of specimens (radiation). DSC was also used to investigate the powders' exothermic effect as their size is reduced during milling (Figures 3 and 4).

TABLE 1. **Chemical composition and basic properties of iron powder.**

Chemical composition (%)							
Lead	**Insoluble in HCL**	**As**	**Cu**	**Mn**	**Sulfide**	**Ni**	**Zn**
0.002	0.05	0.0005	0.005	0.05	0.02	0.05	0.01
Particle size	250-300 mesh						
Purity	99.80%						
Molecular weight	55.85 g						

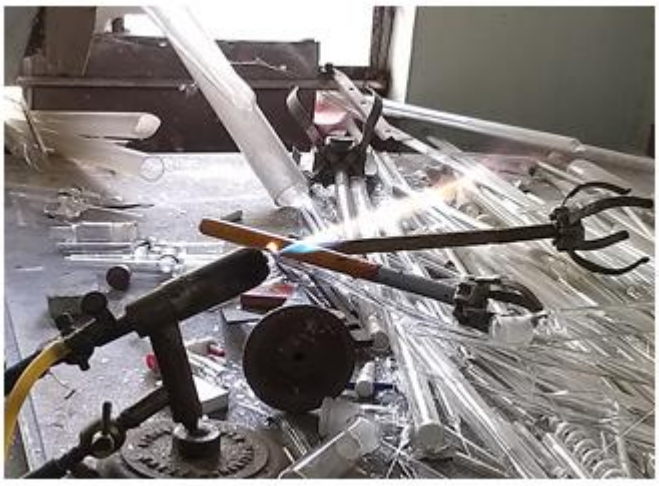

FIG. 3. **Encapsulation through quartz glass blowing.**

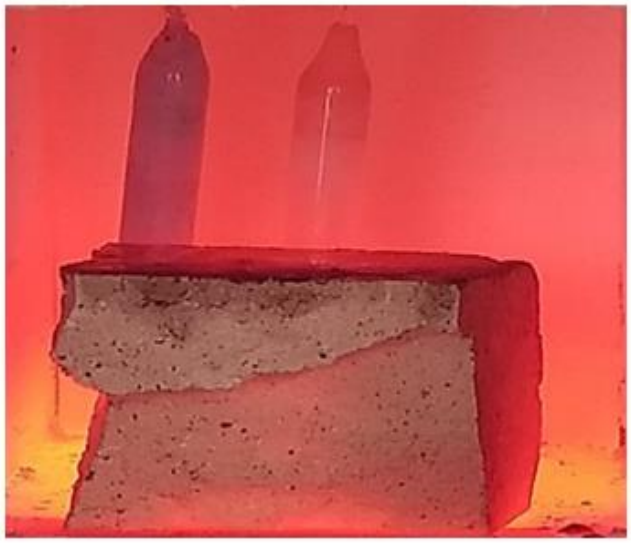

FIG. 4. **Sintering of encapsulated sample in a quartz tube.**

Results and Discussion

Morphology: A digital scanning machine was used to perform SEM on both samples. The shape of pure iron powder milled for 12 hours is shown in Figure 5. The particle size distribution is non-uniform due to the rod shape of the particles. Figures 5 (e) and (f) show some nanosized particles, respectively. There are round, irregular and rod shaped particles, as well as a wide range of particle sizes. After 12 hours of grinding, these particles can be reduced in size from micro to nanoscale.

Figure 6 depicts particle diffusion as a result of sintering. The spaces are filled by atom diffusion during sintering, resulting in the production of these forms. It's also clear that iron granules that come into touch with boron are more compressed than pure iron powders. Boron is added to ferrous alloys formed through the sintering of a persistent liquid eutectic phase of $Fe+Fe_2B$ at 1173°C, which perfectly wets the surface of the base alloy particles. Its dihedral angle is on the order of 10^o or less, thus it wets the iron matrix and easily penetrates the initial interparticle boundaries, but it appears to permeate the grain boundaries with more difficulty or at least more slowly. As a result, powder densification and sinterability improve.

After sintering, the EDS spectra of boron alloyed iron powders are shown in Figure 7. Boron peaks can be seen with iron. The milling media toluene may contribute to carbon intrusion.

Characterization using Xrd: After sintering, the XRD pattern of boron containing iron particles is shown in Figure 8. Multiple iron peaks can be seen in this view. The maximal intensity peak, as is customary, corresponds to the peak of iron. Within a restricted range of two smaller Fe_2B peaks may be detected. At 1173°C, this generates a persistent liquid eutectic phase of $Fe+Fe_2B$, which results in a decrease in interparticle spacing, leading to powder densification. In addition, the Fe_23B_6 chemical appears to be generated with 100% intensity. A strong peak of 100% intensity is also created in some iron carbides. Iron Fe_{23} (B, C) 6 carbide boride is also produced. Fe_2B peaks of varying sizes can also be visible.

Thermal analysis using DSC: The DSC curve of pure iron milled for 3 hours is shown in Figure 9. At temperatures of 775°C and 9700°C, two peaks can be visible. The peak at 775°C is the Curie temperature, which is the temperature at which iron transforms from ferromagnetic to paramagnetic when heated. At 970°C, the phase change of ferrite to the austenite occurs, resulting in a prominent peak in the DSC curve. When cooling down and rerunning the same sample through the same temperature range, this impact is the only one that remains.

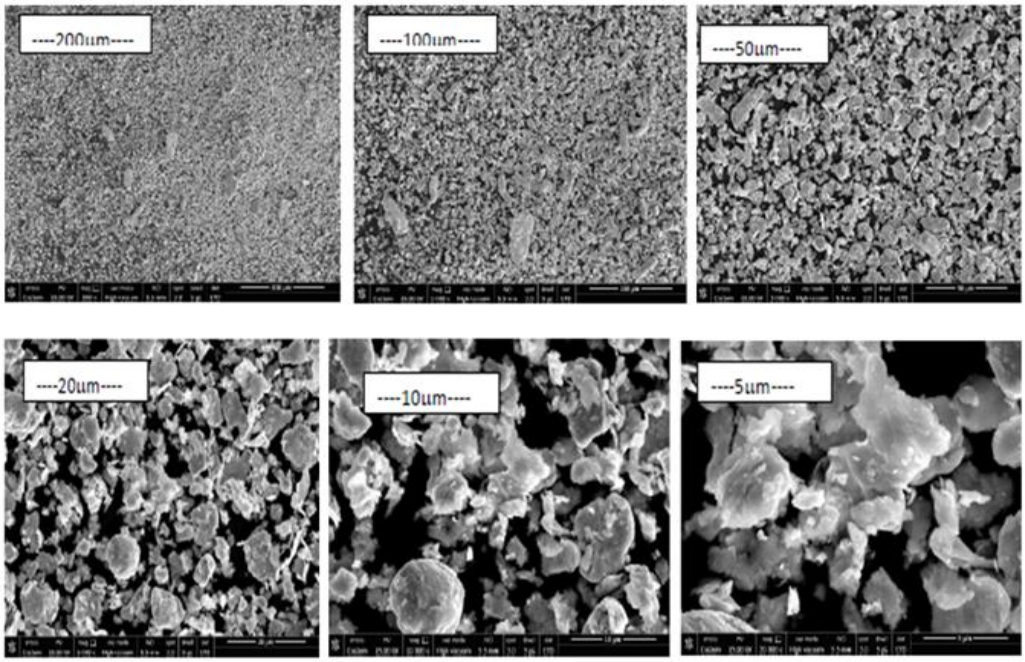

FIG. 5. **SEM micrographs of pure iron after 12 hrs milling at different magnifications.**

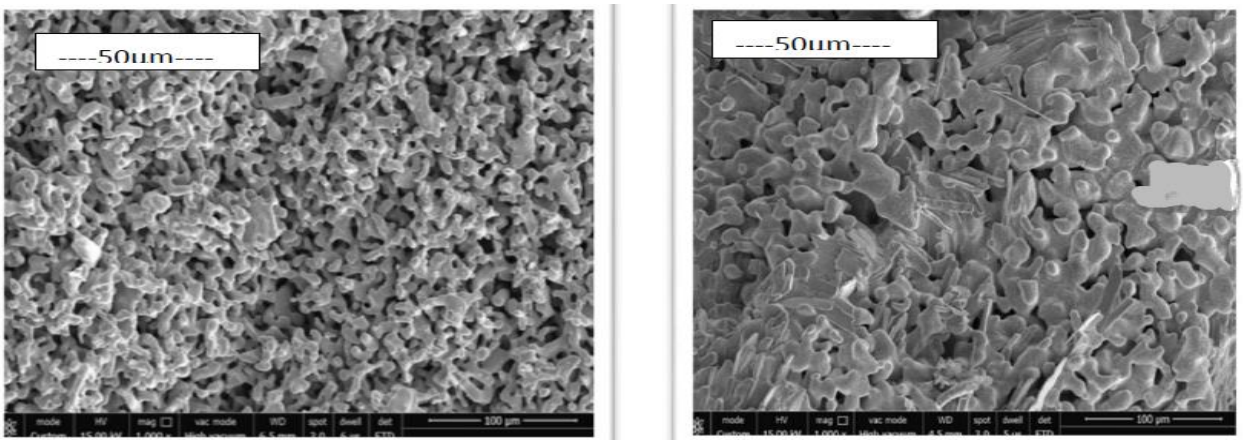

FIG. 6. **This figure shows the micrographs of the sintered pure iron sample and sintered iron boron sample.**

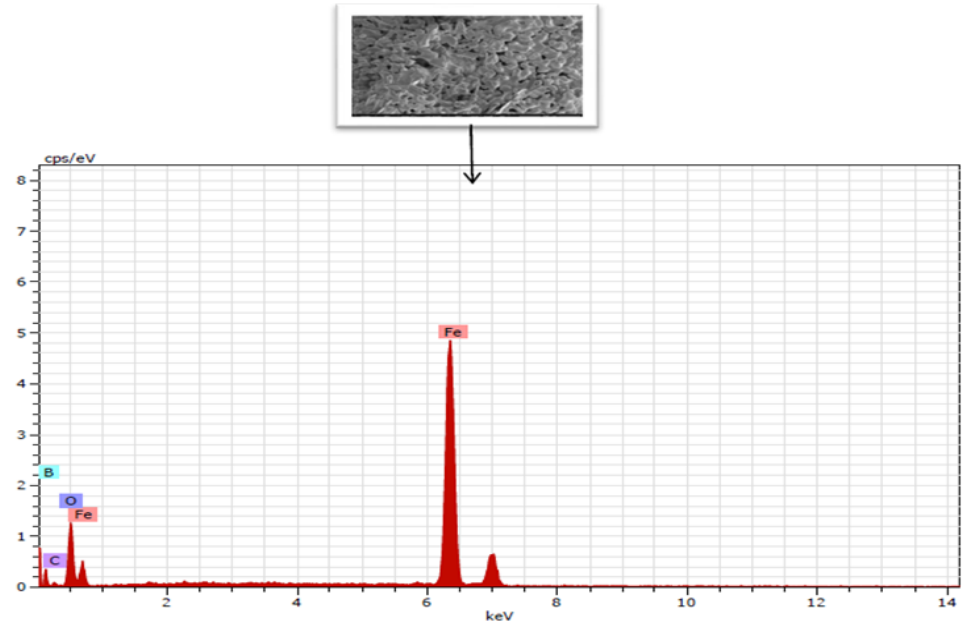

FIG. 7. **EDS spectra of boron containing iron after sintering.**

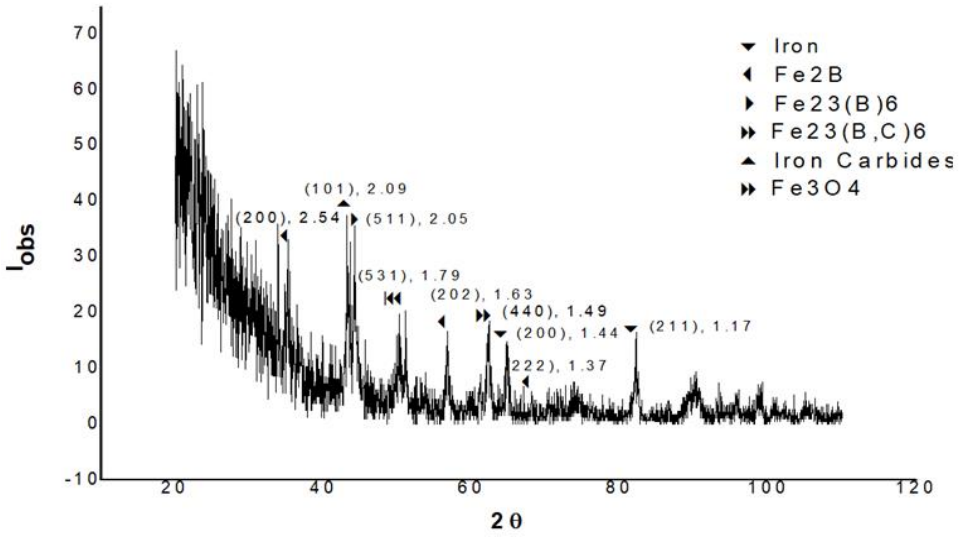

FIG. 8. **X-Ray Diffraction pattern of boron containing iron after sintering.**

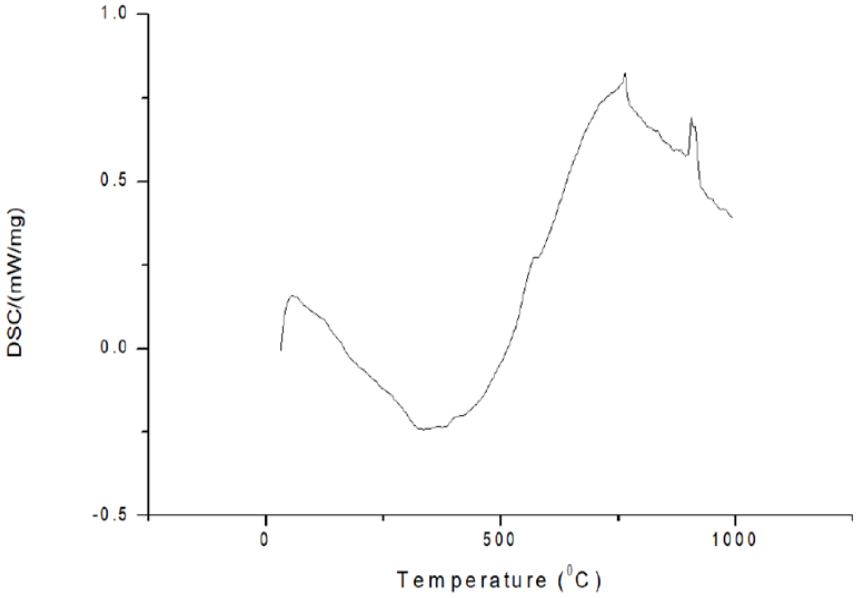

FIG. 9. **DSC curve of pure iron milled for 3 hours.**

The DSC curves at different milling times of 3 hours, 9 hours and 12 hours are shown in Figure 10. With decreasing particle size, the samples demonstrate rising exothermic effects. With decreasing particle size, the peak regions and intensities increase. The surface area of the particle grows as the particle size decreases and the tendency to absorb heat increases, as does the peak area and length.

Figure 11 depicts the displacement of the melting point peak as milling time is increased. In comparison to the melting point peak after 3 hours of milling, the peak after 12 hours of milling has migrated to the left. When the particle size is reduced, the melting point shifts to a lower temperature. The increase in effective surface area is one of the explanations. With the increase in surface area, a bigger portion of the surface will be in touch with the incoming heat, resulting in faster melting.

Within the temperature range of 800°C-1000°C. Figure 12 shows a multitude of peaks of various magnitudes. The creation of some intermetallics can be seen in the endothermic characteristic of the curve shape during cooling. We can deduce the creation of Fe_{23} $(B,C)_6$, $Fe_{23}B_6$ and iron carbides from the XRD examination of sintered iron powder mixed with boron [12-17].

Fe and the intermetallic complex Fe_2B or so called iron boride, are the main phases at all temperatures. The iron base phase with whatever carbon is present as a dissolved solute and Fe_2B are phase relations at high temperatures. The phases are only slightly different at room temperature. They include the iron base phase and either the borocarbide phase, $Fe_{26}(C,B)_6$, which is an intermetallic compound as well or a combination of the borocarbide and Fe_2B [18,19]. The borocarbide phase is the result of a ternary reaction that begins at 9650°C or slightly higher and ends at 8000°C or slightly lower.

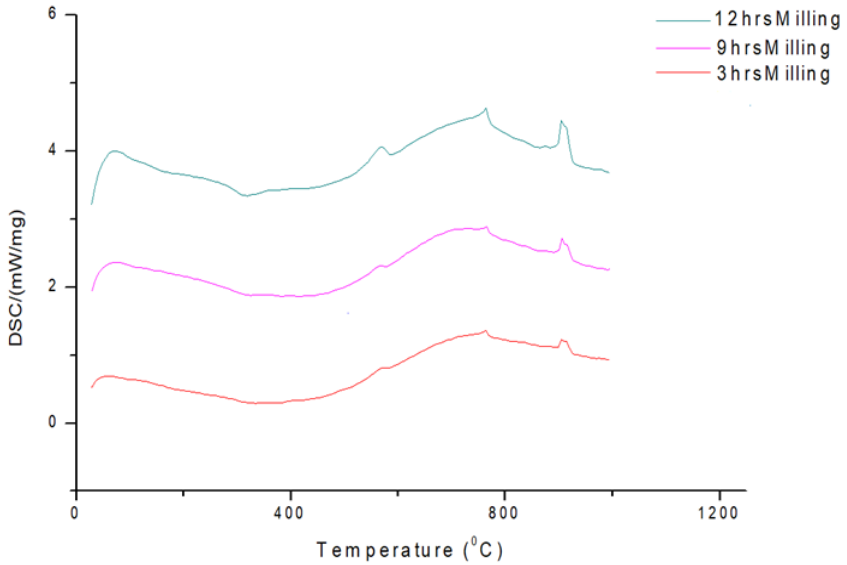

FIG. 10. **DSC curves of pure iron milled at different milling time.**

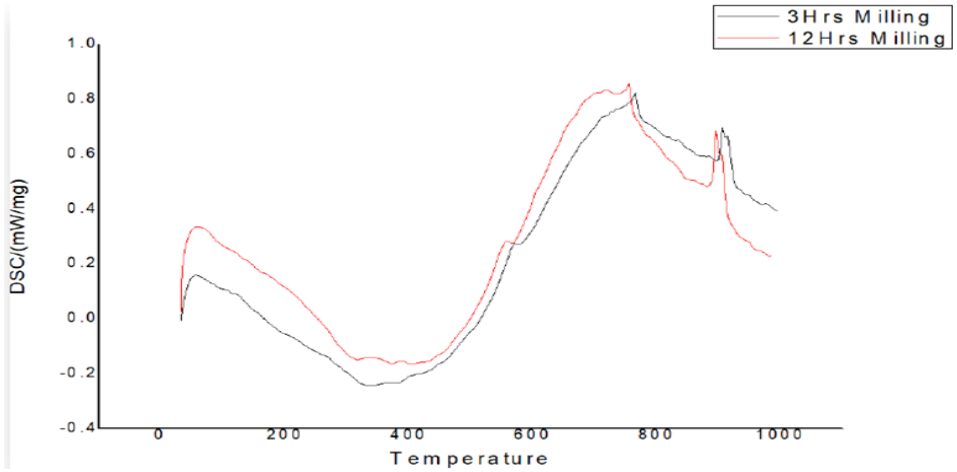

FIG. 11. **Image showing the decrease of melting point with milling.**

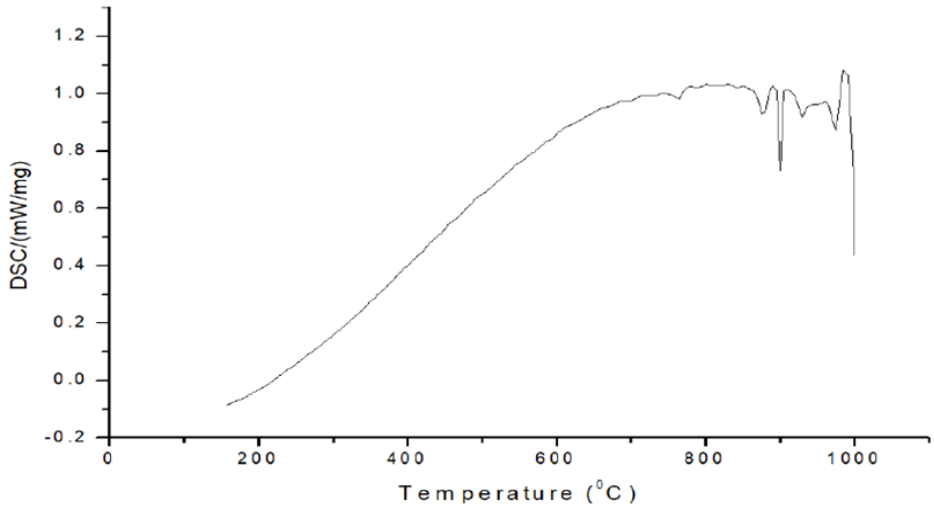

FIG. 12. **Image showing the formation of carbides, borides and borocarbides of iron.**

Because the boron forms a compound that segregates at the grain boundary rather than remaining in the matrix and making it harder, the presence of these borocarbides lowers the sample's hardenability. Boron should be kept in the solution for hardenability because it shifts the pearlitic bay, resulting in the development of harder phases. Furthermore, because these borocarbides provide a low energy channel for crack development, the material becomes brittle. The boron eutectic liquid that caused densification by penetrating the interparticle and grain boundaries is also responsible for the poor characteristics because it persists in the boundaries after cooling and precipitates embrittling intermetallic borides and/or borocarbides. A spheroidizing annealing treatment is the only way to improve things. The method, however, is likely to be costly and the prospective benefits are insufficient to warrant the effort.

Conclusion

The following are some key implications that may be derived from the data presented here:

- When the particle size is reduced, the melting point shifts to a lower temperature. The effective surface area is one of the explanations. As the surface area grows, a larger portion of the surface comes into contact with the temperature, causing melting to occur sooner.
- With decreasing particle size, the samples demonstrate rising exothermic effects. With decreasing particle size, the peak regions and intensities increase. The surface area of the particle grows as the particle size decreases and the tendency to absorb heat increases, as does the peak area and length.
- Sinterability is improved due to grain refining and boron. Boron promoted sintering densification by forming $Fe_{23}(B,C)_6$ and $Fe_{23}B_6$, which have a lower melting point and remain liquid during sintering, reducing the interparticle distance.
- As a result, boron addition will result in increased hardness and abrasion resistance due to the development of harder $Fe_{23}(B,C)_6$, $Fe_{23}B_6$ and iron carbides.
- Because of the larger size reduction, grain development in pure iron may be slower than in mechanically alloyed Fe+B powders.

Conflict of Interest

I/we certify that the publication of this paper is free of financial and non-financial competing interests. I warrant and represent that the work does not infringe on someone else's proprietary or personal rights including, but not limited to, copyrights or privacy rights; that the work is factually true and that it contains no libelous or otherwise unlawful material.

Acknowledgment

Prof. Vijay's insightful and constructive counsel was invaluable during the conception and implementation of this research endeavour and I'd want to express my gratitude to him. It has been tremendously appreciated that he has offered his time so generously. I'd want to thank the technicians at my department's laboratory for helping me get the resources I required to run the software. Finally, I'd like to thank my parents for their constant support and encouragement throughout my academic career.

References

1. German RM. Liquid phase sintering. 1st edition, Springer Publication, New York, United States, 1985.
2. Narasimhan KS. Recent advances in ferrous powder metallurgy. Adv Perform Mater. 1996;3:7-27.
3. Toennes C. Full density sintering by boron addition in a martensitic stainless steel. Adv Powder Metall Part Mater. 1992;3:371-381.
4. Molinari A, Kazior J, Marchetti F, et al. Sintering mechanisms of boron alloyed AISI 316L stainless steel. Powder Metall. 1994;37(2):115-122.
5. Loy B. Effect of boron on some properties of sintered iron carbon alloys. Met Powder Rep. 1984;39:343-346.
6. Park HH, Kwon OJ, Yoon DN. The critical grain size for liquid flow into pores during liquid phase sintering. Metall Trans A. 1986;17:1915-1919.
7. Menapace C, Molinari A, Kazior J, et al. Surface self-densification in boron alloyed austenitic stainless steel and its effect on corrosion and impact resistance. Powder Metall. 2007;50(4):326-335.
8. Lee SM, Kang SJ. Theoretical analysis of liquid phase sintering: Pore filling theory. Acta Mater. 1998;46(9):3191-3202.
9. Menapace C, Molinari A, Kazior J, et al. Surface self-densification in boron alloyed austenitic stainless steel and its effect on corrosion and impact resistance. Powder Metall. 2007;50(4):326-335.
10. Dudrova E, Selecka M, Burea R, et al. Effect of boron addition on microstructure and properties of sintered Fe-1.5 Mo powder materials. ISIJ Int. 1997;37(1):59-64.

11. Cui G, Kou Z. The effect of boron on mechanical behavior and microstructure for Fe-Cr matrix alloy prepared by P/M. J Alloys Compd. 2014;586:699-702.
12. Campos M, Torralba JM, Oro RD, et al. New Opportunities for low alloy steels master alloys for liquid phase sintering. Metals. 2021;11(1):176.
13. Bagliuk G. Properties and structure of sintered boron containing carbon steels. Sinter Methods Prod. 2012.
14. Wu MW, Cai WZ, Lin ZJ, et al. Liquid phase sintering mechanism and densification behavior of boron alloyed Fe-Ni-Mo-CB powder metallurgy steel. Mater Des. 2017;133:536-548.
15. Sulima I. Role of boron addition on the consolidation and properties of steel composites prepared by SPS. Bull Mater Sci. 2015;38:1831-1841.
16. Skalon M, Kazior J. Enhanced sintering of austenitic stainless steel powder AISI 316L through boron containing master alloy addition. Arch Metall Mater. 2012;57(3):789.
17. You J, Hong SH. Densification mechanism and microstructure development of Fe-Ni alloys consolidated by field assisted sintering. J Alloys Compd. 2021;884:161102.
18. Narasimhan KS. Sintering of powder mixtures and the growth of ferrous powder metallurgy. Mater Chem Phys. 2001;67(1-3):56-65.
19. Tardon R, German RM. Sintering and mechanical properties of boron doped austenitic stainless steel. Metal Powder Rep. 1998;12(53):36.